

# Formation mechanism of insensitive tellurium hexanitride with armchair-like cyclo-N<sub>6</sub> anions

Zhao Liu<sup>1</sup>, Da Li<sup>1</sup>  , Quan Zhuang<sup>1</sup>, Fubo Tian<sup>1</sup>, Defang Duan<sup>1</sup> , Fangfei Li<sup>1</sup> & Tian Cui<sup>1,2</sup> 

The lower decomposition barriers of cyclo-N<sub>6</sub> anions hinder their application as high-energy-density materials. Here, first-principles calculations and molecular dynamics simulations reveal that enhancing the covalent component of the interaction between cyclo-N<sub>6</sub> anions and cations can effectively improve the stability of cyclo-N<sub>6</sub> anions. Taking tellurium hexanitride as a representative, the exotic armchair-like N<sub>6</sub> anions of tellurium hexanitride exhibit resistance towards electronic attack and gain extra stability through the formation of covalent bonds with the surrounding elemental tellurium under high pressures. These covalent bonds effectively improve the chemical barrier and insensitivity of tellurium hexanitride during blasting, which prevents the decomposition of solid cyclo-N<sub>6</sub> salts into molecular nitrogen. Furthermore, the high-pressure induced covalent bonds between cyclo-N<sub>6</sub> anions and tellurium enable the high bulk modulus, remarkable detonation performance, and high-temperature thermodynamic stability of tellurium hexanitride.

<sup>1</sup> State Key Laboratory of Superhard Materials, Jilin University, Changchun 130012, People's Republic of China. <sup>2</sup> School of Physical Science and Technology, Ningbo University, Ningbo 315211, People's Republic of China. ✉email: [dali@jlu.edu.cn](mailto:dali@jlu.edu.cn); [cuitian@jlu.edu.cn](mailto:cuitian@jlu.edu.cn)

High pressure, a typically clean and controllable thermodynamic variable, can be adopted to obtain curious materials that are difficult to synthesize under ambient condition<sup>1–3</sup>. Moreover, the precompression evoked by metal elements can reduce the required external pressure for the synthesis of these materials<sup>4</sup>. Under high pressure, metal nitrides have attractive physical and chemical characteristics, such as good superconductivity, good magnetism, good hardness, and a particular catalytic performance<sup>5–8</sup>. Metallic nitrides are conducive to optoelectronic and defect-tolerance characteristics and have strong metal–nitrogen bonds for structural stability and mechanical stiffness<sup>9</sup>. Particularly, the compression of N-rich nitrides has been recommended as an alternative method to obtain metallic atomic nitrogen states as high-energy density materials since the laser-heated diamond anvil cell, which is a powerful tool, has been used to synthesize a series of stable monatomic forms of solid nitrogen<sup>10–13</sup>. Synthesizing pentazolate or  $\pi$ -aromatic ions is considered one of the best and most efficient methods to obtain metallic poly-nitrogen phases<sup>14</sup>. However, all  $\pi$ -aromatics are incredibly unstable, difficult to synthesize, and sensitive to electrophilic attack, and they mostly appear nonmetallic<sup>15</sup>.

Many attempts have been made to synthesize pentazolate anion until cyclo-N<sub>5</sub><sup>−</sup>, and the first attempt was first reported in 1998<sup>16</sup>. Later, the pentazolate salt in solid (N<sub>5</sub>)<sub>6</sub>(H<sub>3</sub>O)<sub>3</sub>(NH<sub>4</sub>)<sub>4</sub>Cl was reported with a stable thermal decomposition temperature (390 K) via thermogravimetric experiments<sup>17,18</sup>. Recently, the controllable and synthetic cyclo-N<sub>5</sub> ionic salt CsN<sub>5</sub> was reported at 60 GPa with a high-energy density and a relatively assessable pressure<sup>19</sup>. Compressing CsN<sub>3</sub> mixed with N<sub>2</sub> cryogenic liquid was also used to achieve cyclo-N<sub>5</sub> ionic salt according to a synchrotron X-ray diffraction measurement at 55.4 GPa in a diamond anvil cell. A Raman spectral vibration mode unique to the cyclo-N<sub>5</sub><sup>−</sup> anion was observed in LiN<sub>5</sub> salt<sup>20</sup>. Because of the intrinsic stability of N<sub>5</sub><sup>−</sup> anions, their crystals have considerable kinetic stability that may be sufficient for an ambient pressure recovery. Considering their electronic structures, the effective separation of the  $\sigma$  and  $\pi$  electrons that correspond to the highest occupied molecular orbital (MO) and lowest unoccupied MO can help to stabilize cyclo-N<sub>5</sub><sup>−</sup>/N<sub>5</sub><sup>+</sup> salt<sup>21</sup>. Likewise, the pursuit of energy-intensive cyclo-N<sub>6</sub> salts with higher nitrogen contents than pentazolate anions, which are synthesized at a modest pressure, has never ceased<sup>22</sup>. However, the cyclo-N<sub>6</sub> ionic salt only remains in the theoretical stage. Numerous planar or quasi-planar cyclo-N<sub>6</sub> anions are predicted at high pressure in Li, Mg, Cs, Ca, Rb, and Ba nitrides, but they have not been successfully synthesized for unclear reasons<sup>6,22–25</sup>.

These theoretical studies did not pay close attention to the microstructural characteristics of cyclo-N<sub>6</sub> anions. It is of note that an in-plane distortion may occur in cyclo-N<sub>6</sub> sub-lattices when the neutral  $\pi$ -aromatic switches to a charged anion. For instance, armchair-like N<sub>6</sub> rings are predicted in  $h$ -W<sup>2.4+</sup>N<sub>6</sub><sup>2.4–26</sup>. Once a benzene-like molecule forms a cyclo-N<sub>6</sub><sup>6−</sup> anion, its symmetry reduces and even decomposes because its antibonding states are fully occupied, which may prevent experimental synthesis. Another reason may be that the decomposition barrier of cyclo-N<sub>6</sub> anions is extremely low and they spontaneously decompose to other anions. We propose a strategy to maintain the “non-molecular nitrogen phase”, i.e., to enhance its energy barrier and insensitivity via covalent bonds entrapment between metal/non-metal and cyclo-N<sub>6</sub> ions to keep it from breaking down into the molecular phase. Based on these judgments, armchair-like cyclo-N<sub>6</sub> anions may be able to be stabilized if their antibonding MOs are not completely occupied and their structures are entrapped by covalent effects. Considering that Te has higher electronegativity and a larger atomic radius than W, it easily forms covalent bonds

with nitrogen; thus, we adopt the binary Te–N candidates as prototypes to search for cyclo-N<sub>6</sub> ions and study the trap effect by the covalent bond<sup>27,28</sup>.

In this work, our broad structure searches combined with first-principles simulations identify a TeN<sub>6</sub> nitride with armchair-like cyclo-N<sub>6</sub> anions, high-pressure–temperature stability and remarkable mechanical properties. Herein, tellurium serves as an electron donor to modulate the electronic distribution and forms covalent bonds with nitrogen atoms, which induces metallic cyclo-N<sub>6</sub> anions. Meanwhile, covalent bond entrapment to stabilize the armchair-like cyclo-N<sub>6</sub> anions is revealed. More importantly, the covalent bonds effectively improve the chemical barrier and insensitivity to prevent the decomposition of monatomic forms of solid N<sub>6</sub> anions into the molecular phase. Moreover, the detonation performance and energy density of the metallic cyclo-N<sub>6</sub> anions predicted by our study are higher than those of most previously reported pentazolate and six-membered N<sub>6</sub> anions in binary nitrides.

## Results and discussion

**Phase stability and structural features at high pressure.** A neutral cyclo-N<sub>6</sub> molecule with inherent benzene-like structure has planar D<sub>6h</sub> symmetry<sup>29</sup>. However, the crystalline sub-lattice N<sub>6</sub> isolated anions have D<sub>3d</sub> symmetry in the anti-CdCl<sub>2</sub> TeN<sub>6</sub> phase (space group *R*-3*m*, Supplementary Table 1) because of structural mutations, as shown in Fig. 1a and Supplementary Fig. 1. The armchair-like structural configuration of the equivalent bonding in 3D space hints that the nitrogen atoms adopt  $sp^3$  hybridization to form  $\sigma$  covalent bonds. The distance between nitrogen atoms is 1.37 Å at million magnitude pressure, which is a prototypical N–N single bond without the resonance effect between alternating  $\pi$ - and  $\sigma$ -bonds. After removing tellurium atoms from the anti-CdCl<sub>2</sub> phase, as shown in Fig. 1b, the cyclo-N<sub>6</sub> structure transforms into a flat shape with D<sub>6h</sub> symmetry but remains in the anti-CdCl<sub>2</sub> phase. Compared with the anti-CdCl<sub>2</sub>-TeN<sub>6</sub> phase, the volume of planar cyclo-N<sub>6</sub> decreases by 20%, which suggests that the structural deformation of cyclo-N<sub>6</sub> is related to the interactions with tellurium atoms. Thus, the N–N bond lengths, Bader charge transfer and volumes as functions of pressure are analyzed to gain insight into the interaction between atoms. The volume decreases by 0.20 Å<sup>3</sup>/GPa almost linearly with pressure, which indicates strong incompressibility, as shown in Supplementary Fig. 2, while the charge transfer amount gradually increases, as shown in Fig. 1c. However, the change in the N–N distances under high pressure is extremely weak, which preserves N–N single bonds. Herein, the decrease in lattice volume under pressure is mainly attributed to the Te–N distance shrinkage, which increases the interaction and stimulates new physico-chemical properties.

The possible routes and pressures for synthesizing anti-CdCl<sub>2</sub> phase are summarized and displayed in Fig. 1d. The N–N single bonds endowed TeN<sub>6</sub> with superior energy storage properties, which reached 4.79 kJ/g after decomposing into pollution-free nitrogen and the P<sub>3</sub>,21-Te phase. The average N–N displacements of the anti-CdCl<sub>2</sub> phase at 500 and 1000 K after the 50 Ps first-principles molecular dynamics (AIMD) simulations shown in Fig. 2a are still 1.37 Å, which suggests that the structural framework remains basically unchanged and thermodynamically stable. The radial distribution function  $g(r)$  (Fig. 2b) confirms that the covalent N–N single bonds retained in an isolated peak in cyclo-N<sub>6</sub> anions were not broken, and the long-range order naturally persists to crystallize even at temperatures up to 1000 K<sup>30</sup>. The phonon dispersion calculation demonstrates mechanical stability as shown in Supplementary Fig. 3. The mechanical natures are identified in Supplementary Table 3. Especially, the

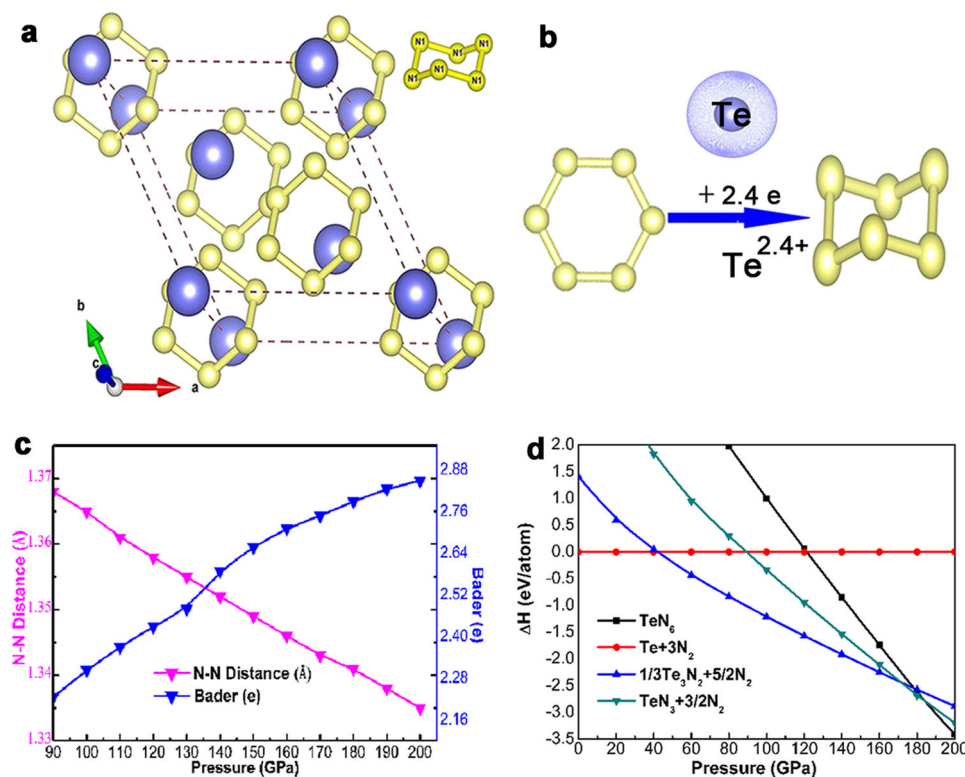


**Fig. 1** Structural properties and enthalpies of  $\text{TeN}_6$  under high pressures. **a** Stable structures of the anti- $\text{CdCl}_2$  phase at 120 GPa. **b** Planar cyclo- $\text{N}_6$  sub-lattice interacted with Te atoms to form armchair-like  $\text{N}_6$  anions. **c** N-N bond lengths and Bader charge transfer as a function of pressure in  $\text{TeN}_6$ . **d** Enthalpy of the anti- $\text{CdCl}_2$  phase relative to the mixture of  $P3_121$ -Te, TeN or  $\text{TeN}_3$  and the  $P4_12_12$  nitrogen phases.

bulk modulus of the anti- $\text{CdCl}_2$  phase is 505 GPa higher than that of diamond 431 GPa<sup>31</sup>, which implies a larger volume compression resistance and covalent bonds equipment. An evidently high value of  $C_{33}$  (929 GPa) is attached to the crystal, which identifies its remarkable high stiffness along the  $c$ -axis. The remarkable mechanical properties enable metallic  $\text{TeN}_6$  to better resist external force destruction under extreme conditions.

**Electronic structure and bonding properties.** Compared with the neutral planar cyclo- $\text{N}_6$  sub-lattices in the  $R3m$ - $\text{N}_6$  phase, the structural deformation induced by tellurium atoms is subject to the Jahn-Teller effect in the anti- $\text{CdCl}_2$   $\text{TeN}_6$  phase. A typical symmetry breakage occurs because its geometries with high symmetry produce real or approximate degenerate states. In Fig. 3b, the degeneracy of the  $p_x$  and  $p_y$  orbitals in the  $R3m$ - $\text{N}_6$  phase is obvious near the Fermi level. However, along the K- $\Gamma$ ,  $\Gamma$ -M, M-L, and L-H directions, the corresponding MOs (red lines) are nondegenerated in the anti- $\text{CdCl}_2$   $\text{TeN}_6$  phase and extend in the direction of lower energy. Then, structural distortion inevitably cause changes in the physical properties. The anti- $\text{CdCl}_2$   $\text{TeN}_6$  exhibiting metallic property is a sharp contrast to the insulator properties in the  $R3m$ - $\text{N}_6$  phase. The dispersion of the  $\text{N}_p$  orbitals increases with the strong interaction with tellurium atoms, and a Van Hove singularity is formed near the Fermi level, as shown in Fig. 3a. The consistency of the Te- and N- $p$  orbital profiles shown in Supplementary Fig. 4 confirms the  $sp^3$  hybridization. In general, the nonplanar cyclo- $\text{N}_6$  can inhibit the delocalization effect of  $\pi$  electrons, which should be a nonmetallic state<sup>32</sup>. Thus, tellurium atoms play critical roles in bonding and metallic properties for cyclo- $\text{N}_6$  anions except for causing structural deformation. Consequently, we perform Crystal orbital

Hamilton population (COHP) quantitative analysis, as shown in Fig. 4a, to identify the role of tellurium atoms in the bonding interaction with cyclo- $\text{N}_6$ . Intriguingly, the tellurium atom serves as an excellent reductant in ionic crystals and forms an unusual covalent bond with the adjacent cyclo- $\text{N}_6$  since the integral COHP (ICOHP) value ( $\text{N1-Te1}^a$ , nearest neighbor distance) reaches  $-0.64$  eV and the sub-adjacent ( $\text{N1-Te1}^b$ , second nearest neighbor distance) is  $-0.35$  eV, which implies an overlap of their electron clouds. Meanwhile, this finding proves that Te atoms (in a formula unit, f.u.) do not completely transfer all the valence electrons ( $6e$ ) into the antibonding  $\psi^*$  ( $\text{N-}p_z$ ) MOs, as shown in Fig. 4b. This result is also confirmed by the Bader charge analysis, which reveals that the charge from one Te atom to one  $\text{N}_6$  ring is approximately  $2.4e$ . Then, we analyze the metallization process in detail from the perspectives of cyclo- $\text{N}_6$  and Te MOs. The cyclo- $\text{N}_6$  unit inherently has six  $\pi$  MOs ( $P_z$ ) and  $\pi$  electrons: three bonding  $\psi_{1-3}$  and three antibonding  $\psi_{4-6}^*$  MOs. Assuming that no electron transfer occurs, three bonding  $\psi_{1-3}$  MOs are occupied, while the higher-energy antibonding MOs  $\psi_{4-6}^*$  remains vacant and exhibit nonmetallic properties. Considering the interactions with the Te atoms, each  $\psi$  MO produces a scattered  $\pi$  band along  $\Gamma$ -A and K-M in the Brillouin region and induces the band overlap and metallic phenomenon. Meanwhile, the Te 5p electron, as shown in Supplementary Fig. 4, is completely delocalized in this phase, so it has a strong influence on the electronic structures of  $\text{TeN}_6$  except for lowering the Fermi level and plays a relatively significant role in the conducting behavior, which is in strong contrast to Heusler semiconductors<sup>33</sup>.

We further investigated the covalent bond effect of cyclo- $\text{N}_6$  anions. Through the topological analysis of the coupling electron charge density with Laplacian, the bond critical points (BCPs) derived from a QTAIM<sup>34</sup> were adopted to further confirm the

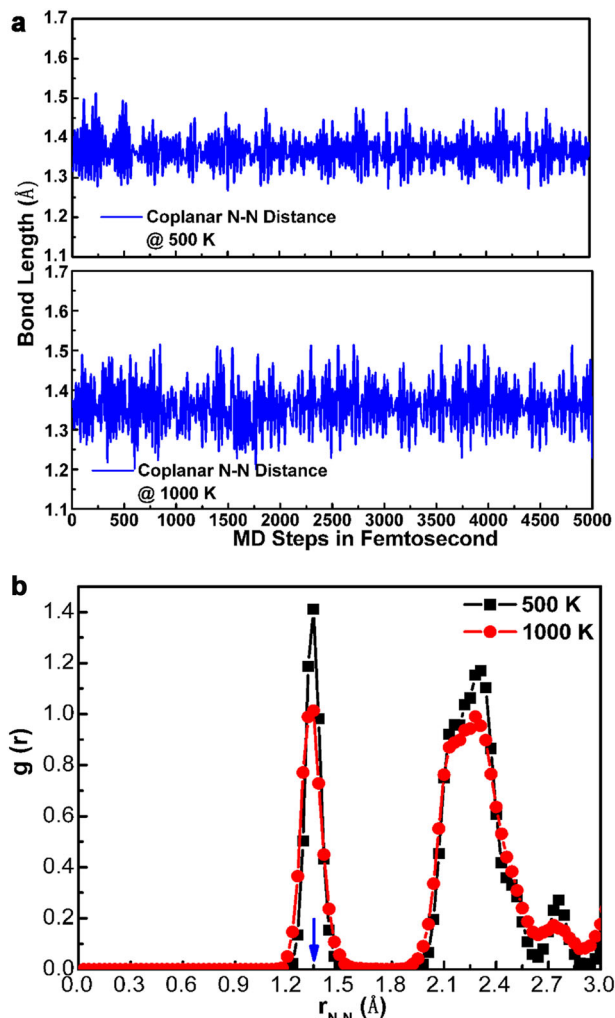


**Fig. 2 N-N displacements and radial distribution function.** **a** N-N bond lengths as a function of time and **b** radial distribution function  $g(r)$  at 500 and 1000 K under a constant pressure (120 GPa) according to AIMD simulations. The blue arrow denotes the N-N single bond distance according to the previous report.

bonding behavior, as shown in Fig. 4c. In the (001) plane, the solid isovalues of Laplace for its electron density at BCP are negative, which indicates strong covalent interactions. N atoms connect to the nearest neighbors and form bond paths. The nearest Te and N atoms also have negative isovalues of Laplacian; the actual effect between them is due to polar covalent bonds but not entirely of the closed-shell interaction category<sup>35</sup>. Each Te covalently bonds with six  $N_6$  units, while each N in  $sp^3$  hybridization forms three covalent bonds (one Te and two N atoms), which implies that Te can form abundant delocalized chemical bonds. The three-dimensional structure formed by the effective covalent bonds endows metallic  $TeN_6$  with higher hardness ( $H_V$ , 24 GPa), as shown in Supplementary Table 3. Meanwhile, the bonding configuration of  $cyclo-N_6$  changes from  $AX_2E_2$  in isolated  $N_6$  ions to  $AX_3E_1$  (Fig. 4d and Supplementary Fig. 5), which effectively restrains the damage caused by the interactions of nonbonding pairs to the system's stability<sup>36</sup>. In addition to the electrostatic interaction between  $Te^{2.4+}$  and  $N_6^{2.4-}$  ions, which reduces the energy by forming strong ionic bonds, the existence of weak covalent bonds leads to the same function since the COHP integral of Te-N leads to a drop of approximately  $-1$  eV/f.u. of the MO energy.

**Chemical insensitivity and detonation performance.** Nitrides are unstable energy-intensive materials and are expected to be highly insensitive, which allows their use in detonation applications<sup>15</sup>. The discovered Te-N covalent bonds led us to investigate their energy barrier. According to the ICOHP calculation of the Te-N bonds, the potential barrier induced by the covalent bond is 96.49 kJ/mol per f.u., as shown in Fig. 5, which accounts for most of the tellurium mixing energy barriers (129.80 kJ/mol), and plays an important role in improving the chemical barrier and insensitivity property. Moreover, the study of the stability of arylpentazoles indicates that the potential barriers of their various compounds are 78–100 kJ/mol, which are lower than the predicted potential barriers of  $cyclo-N_6$  in our report<sup>37</sup>. As is known, a large pressure is required to overcome the energy barrier ( $\sim 82.98$  kJ/mol) of dinitrogen  $N_2$  to shape the polynitrogen phase during synthesis. A higher barrier induced by covalent bonds can resist the spontaneous decomposition of  $cyclo-N_6$ . In contrast, for the known quasi-planar  $cyclo-N_6^{2-}$  anions in the  $C2/m$ - $CsN_3$  phase (Supplementary Fig. 6 and Supplementary Table 1), covalent interactions did not occur between cesium and  $cyclo-N_6$  anions since all the ICOHP values presented in Supplementary Table 2 are greater than 0. However, the armchair-like  $cyclo-N_6$  in  $h$ - $WN_6$  has covalent bond characteristics, which shows that armchair-like  $N_6$  anions have extra stability and prevent the decomposition of the monatomic forms of solid  $cyclo-N_6$  ions into molecular phases.

The detonation performance estimated by the Kamlet–Jacobs empirical equations is one of the most important indicators of energetic materials<sup>38</sup>. The detonation performances of traditional high-energy-density materials, e.g., TNT and RDX, are shown in Supplementary Table 4, and detailed descriptions are provided in Supplementary Note 1<sup>39</sup>. The  $cyclo-N_6$  anions that release a large amount of nitrogen are considered environmental friendly clean energetic materials. According to the principle of maximum heat release, the detonation products are determined to be tellurium and nitrogen under ambient conditions. Herein, the gravimetric energy loading density of  $TeN_6$  was calculated to be approximately 8.16 g/cm<sup>3</sup>. We estimated the detonation velocity ( $D$ ) and detonation pressure ( $P$ ) using decomposition products at ambient pressure. Intriguingly, due to the dual effects of its high-energy density and loading density, its detonation pressure is four times greater than that of traditional TNT and two times greater than that of pentazolate anion in  $MgN_{10}$  salt<sup>40,41</sup>.

In summary, we report an armchair-like  $cyclo-N_6$  anion salt with an inherent single covalent bond through swarm-intelligence structure searches of the  $TeN_6$  system. The covalent bond modifies the distribution density of local electron clouds and effectively increases the kinetic energy, which is an important factor for metallization in the  $TeN_6$  structure. More importantly, the armchair-like  $cyclo-N_6$  anion can be stabilized by additional covalent bond entrapment, which effectively improves the chemical barrier and insensitivity. In addition, the energy density of  $cyclo-N_6$  anions is higher than that of multitudinous pentazolate and six-membered anions under high pressure in binary nitrides. The simulated detonation performance of the armchair-like  $cyclo-N_6$  anion salt is much higher than that of traditional TNT/RDX blasting materials. This study is important regarding the insensitivity of  $cyclo-N_6$  anions and may facilitate high-pressure synthesis.

## Methods

**Structure search.** The predicted crystalline phases are based on the global minimization of energy surface merging particle swarm optimization methodology as actualized in the CALYPSO code<sup>42</sup>. The favorite structures of tellurium nitride were predicted at 0, 20, 50, 100, 150, and 200 GPa using the simulation cell, which consisted of 2–4 f.u.

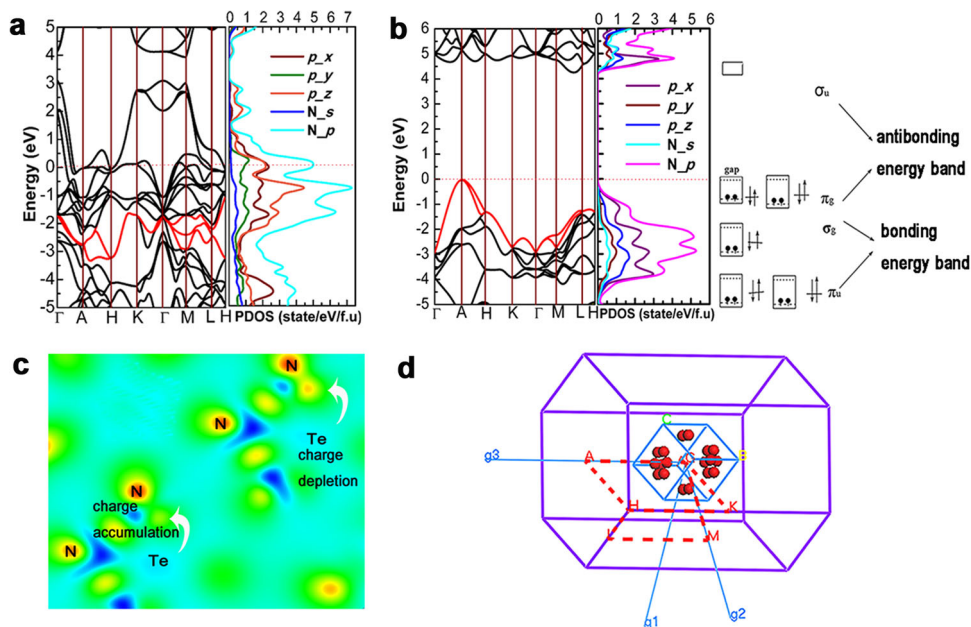


**Fig. 3 Electronic structure and differential charge density analysis.** **a** Electronic band structures and projected density of states (PDOS) with  $\text{TeN}_6$ . **b** Planar six-membered  $\text{N}_6$  optimized after removing Te atoms at 120 GPa and its schematic molecular orbital diagram for N atoms. **c** Differential charge density of  $\text{TeN}_6$  projected on the  $(-0.5, 0.6, 0.7)$  plane. **d** Selected high symmetry point and path in the reciprocal lattice space to calculate the energy bands.

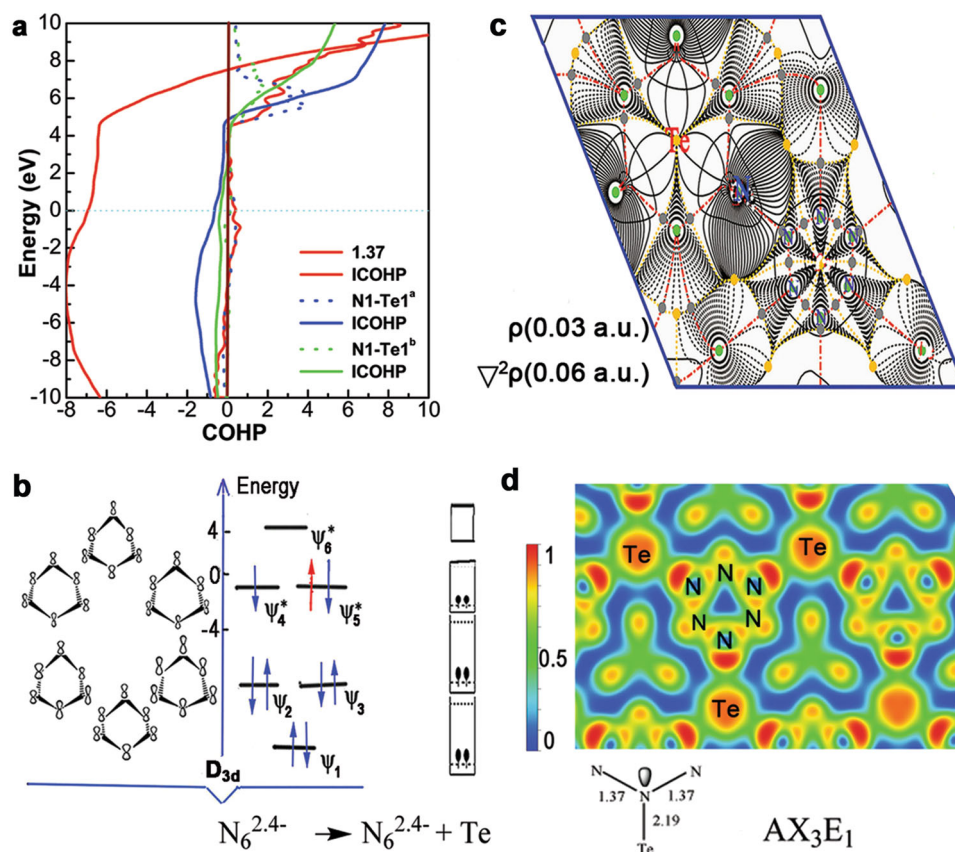


**Fig. 4 Bonding characteristics under high pressure.** **a** Plot of COHP and ICOHP for anti- $\text{CdCl}_2$ -type  $\text{TeN}_6$  at 120 GPa. **b** Simplified correlation diagram of the  $p_z$  orbitals of cyclo- $\text{N}_6$  and the schematic orbital overlap of  $\text{N}_6^{2.4-}$  MOs, which form because of tellurium. **c** Gradient paths and critical points derived from a QAIM analysis in the (001) plane. The heavy, dotted, and solid thin lines correspond to the zero, positive, and negative isovalues of Laplacian, respectively. **d** Electron localization functions in the (001) plane and bonding features marked by the VSEPR notation.

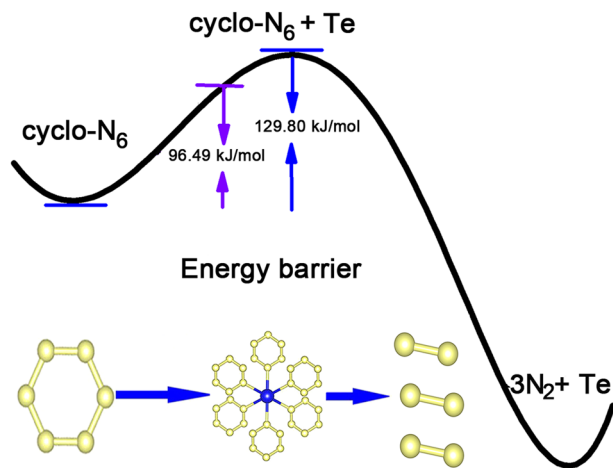


**Fig. 5** Stabilization of the cyclo-N<sub>6</sub> anion by covalent bonds entrapment.

Tellurium mixing enhances the insensitivity of the cyclo-N<sub>6</sub> anion by improving the energy barriers by 129.80 kJ/mol per f.u.; the potential barrier induced by the covalent bond is 96.49 kJ/mol per f.u. relative to the isolated cyclo-N<sub>6</sub> in the stability effect.

**Electronic structure and total energy calculations.** Density functional theory in the Perdew–Burke–Ernzerhof parameterization of the generalized gradient approximation as implemented in the Vienna ab initio simulation (VASP) code was employed for the relaxations<sup>43–45</sup>. Van der Waals (vdW-DF2) interactions were used to correct the structural rationality<sup>46</sup>. The projector-augmented wave method was utilized with the Te and N potentials, where  $5s^25p^4$  and  $2s^22p^3$  were considered valence electrons. A plane-wave (PW) basis set cutoff of 850 eV and a Monkhorst–Pack  $k$  meshes spacing of  $2\pi \times 0.03 \text{ \AA}^{-1}$  were used; the self-consistent field tolerance was of  $0.1 \times 10^{-5} \text{ eV/atom}$ . The COHP analyses executed in the LOBSTER code<sup>47</sup> were performed for the TeN<sub>6</sub> compound to elucidate its bonding information. To provide detailed information, the COHP was calculated based on the PW method and was performed by re-extracting atom-resolved information from the delocalized PW basis sets<sup>48</sup>. Based on counted energy-weighted population of the wave functions between two atomic orbitals, the ICOHP value quantitatively represented the covalent bonding strength. In addition, the phonon calculations were performed using a supercell approach in the finite displacement theory as implemented in the PHONOPY code<sup>49</sup>.

**Molecular dynamics simulation.** We also performed a first-principles molecular dynamics simulation to determine the thermal stability of the anti-CdCl<sub>2</sub> structure via NPT ensembles (N is particle number, P is pressure, and T is temperature). The 84 nitrogen atoms in the super-lattice were used. Molecular dynamics calculations were performed at temperatures of 500 and 1000 K, each of which included 5000 1-fs time steps. Referring to the previous analysis, we generally reached a consensus that the bond lengths of the single bond, double bond, and triple bond were 1.45, 1.25, and 1.10 Å, respectively, under ambient conditions. The N–N single bond distance in cg-N is 1.31 Å at 200 GPa<sup>6</sup>, which can guide the assignment of N–N bonds to rationalize the local structural environments with the VSEPR theory.

## Data availability

The data supporting this publication are available from the authors on request.

Received: 17 December 2019; Accepted: 9 March 2020;

Published online: 02 April 2020

## References

- Pickard, C. J. & Needs, R. J. High-pressure phases of nitrogen. *Phys. Rev. Lett.* **102**, 125702 (2009).
- Eremets, M. I., Gavriluk, A. G., Trojan, I. A., Dzivenko, D. A. & Boehler, R. Single-bonded cubic form of nitrogen. *Nat. Mater.* **3**, 558–563 (2004).
- Ma, Y. M., Oganov, A. R., Li, Z., Xie, Y. & Kotakoski, J. Novel high pressure structures of polymeric nitrogen. *Phys. Rev. Lett.* **102**, 065501 (2009).
- Ashcroft, N. W. Hydrogen dominant metallic alloys: high temperature superconductors? *Phys. Rev. Lett.* **92**, 187002 (2004).
- Peng, F., Yao, Y., Liu, H. & Ma, Y. M. Crystalline LiN<sub>5</sub> predicted from first-principles as a possible high-energy material. *J. Phys. Chem. Lett.* **6**, 2363–2366 (2015).
- Huang, B. & Frapper, G. Barium–Nitrogen phases under pressure: emergence of structural diversity and nitrogen-rich compounds. *Chem. Mater.* **30**, 7623–7636 (2018).
- Liu, Z. et al. Metallic and anti-metallic properties of strongly covalently bonded energetic AlN<sub>5</sub> nitrides. *Phys. Chem. Chem. Phys.* **21**, 12029–12035 (2019).
- Li, X. et al. Hard BN clathrate superconductors. *J. Phys. Chem. Lett.* **10**, 2554–2560 (2019).
- Sun, W. et al. A map of the inorganic ternary metal nitrides. *Nat. Mater.* **18**, 732–739 (2019).
- Zhu, H. et al. Pressure-induced series of phase transitions in sodium azide. *J. Appl. Phys.* **113**, 033511 (2013).
- Li, D. et al. Pressure-induced phase transitions in rubidium azide: studied by in-situ x-ray diffraction. *Appl. Phys. Lett.* **105**, 071903 (2014).
- Jiang, J. et al. Effect of pressure on 4-toluenesulfonyl azide studied by Raman scattering and synchrotron X-ray diffraction. *J. Phys. Chem. C* **121**, 1032–1039 (2017).
- Laniel, D. et al. Synthesis of magnesium-nitrogen salts of polynitrogen anions. *Nat. Commun.* **10**, 4515 (2019).
- Wang, P., Lin, Q., Xu, Y. & Lu, M. Pentazole anion cyclo-N<sub>5</sub><sup>−</sup>: a rising star in nitrogen chemistry and energetic materials. *Sci. China Chem.* **61**, 1355–1358 (2018).
- Zhang, L. et al. Stabilization of the dual-aromatic cyclo-N<sub>5</sub><sup>(−)</sup> anion by acidic entrapment. *J. Phys. Chem. Lett.* **10**, 2378–2385 (2019).
- Christe, K. O. Recent advances in the chemistry of N<sub>5</sub><sup>+</sup>, N<sub>5</sub><sup>−</sup> and high-oxygen compounds. *Propellants Explos. Pyrotech.* **32**, 194–204 (2007).
- Zhang, C. et al. Synthesis and characterization of the pentazole anion cyclo-N<sub>5</sub><sup>−</sup> in (N<sub>5</sub>)<sub>6</sub>(H<sub>3</sub>O)3(NH<sub>4</sub>)4Cl. *Science* **355**, 374–376 (2017).
- Huang, H. et al. Reconciling the debate on the existence of pentazole HN<sub>5</sub> in the pentazolate salt of (N<sub>5</sub>)<sub>6</sub>(H<sub>3</sub>O)3(NH<sub>4</sub>)4Cl. *J. Am. Chem. Soc.* **141**, 2984–2989 (2019).
- Steele, B. A. et al. High-pressure synthesis of a pentazolate salt. *Chem. Mater.* **29**, 735–741 (2017).
- Laniel, D., Weck, G., Gaiffe, G., Garbarino, G. & Loubeyre, P. High-pressure synthesized lithium pentazolate compound metastable under ambient conditions. *J. Phys. Chem. Lett.* **9**, 1600–1604 (2018).
- Moran, N., Shmuel, Z. & Yehuda, H. Stability of polynitrogen compounds: the importance of separating the  $\sigma$  and  $\pi$  electron systems. *J. Phys. Chem. A* **113**, 7376–7382 (2009).
- Prasad, D. L. V. K. & Ashcroft, N. W., & Hoffmann R. Evolving structural diversity and metallicity in compressed lithium azide. *J. Phys. Chem. C* **117**, 20838–20846 (2013).
- Wang, X. et al. Layered polymeric nitrogen in RbN<sub>3</sub> at high pressures. *Sci. Rep.* **5**, 16677 (2015).
- Wei, S. et al. Alkaline-earth metal (Mg) polynitrides at high pressure as possible high-energy materials. *Phys. Chem. Chem. Phys.* **19**, 9246 (2017).
- Zhu, S. et al. Stable calcium nitrides at ambient and high pressures. *Inorg. Chem.* **55**, 7550–7555 (2016).
- Xia, K. et al. A novel superhard tungsten nitride predicted by machine-learning accelerated crystal structure search. *Sci. Bull.* **63**, 817–824 (2018).
- Yu, H., Lin, X., Li, K. & Chen, Y. Unveiling a novel, cation-rich compound in a high-pressure Pb–Te binary system. *ACS Cent. Sci.* **5**, 683–687 (2019).
- Klapotke, T. M., Krumm, B., Mayer, P. & Schwab, I. Binary tellurium(IV) azides: Te(N<sub>3</sub>)<sub>4</sub> and [Te(N<sub>3</sub>)<sub>3</sub>]. *Angew. Chem.* **42**, 5843–5846 (2003).
- Ohanessian, G., Hiberty, P. C., Lefour, J. M., Flament, J. P. & Shaik, S. S. Is delocalization a driving force in chemistry? First- and second-row heteroannulenes. *Inorg. Chem.* **27**, 2219–2224 (1988).
- Liu, H. & Ma, Y. M. Proton or deuteron transfer in phase IV of solid hydrogen and deuterium. *Phys. Rev. Lett.* **110**, 025903 (2013).
- Zhang, M. L. et al. Superhard BC(3) in cubic diamond structure. *Phys. Rev. Lett.* **114**, 015502 (2015).
- Shaik, S., Shurki, A., Danovich, D. & Hiberty, P. C. A different story of  $\pi$ -delocalizations: the distortivity of  $\pi$ -electrons and its chemical manifestations. *Chem. Rev.* **101**, 1501–1539 (2001).
- He, J., Xia, Y., Naghavi, S. S., Ozolins, V. & Wolverton, C. Designing chemical analogs to PbTe with intrinsic high band degeneracy and low lattice thermal conductivity. *Nat. Commun.* **10**, 719 (2019).
- Vega, D., Almeida, D., Ruetter, F., Sierralta, A. & Sánchez, M. AIM-UC: an application for QTAIM analysis. *J. Comput. Methods Sci. Eng.* **14**, 131–136 (2014).
- Song, X. Q. et al. Exotic hydrogen bonding in compressed ammonia hydrides. *J. Phys. Chem. Lett.* **10**, 2761–2766 (2019).
- Gillespie, R. J. The valence-shell electron-pair repulsion (VSEPR) theory of directed valency. *J. Chem. Educ.* **40**, 295–301 (1963).

37. Jiao, F. & Zhang, C. Origin of the considerably high thermal stability of cyclo- $N_5^-$  containing salts at ambient conditions. *Cryst. Eng. Comm.* **21**, 3592–3604 (2019).
38. Kamlet, M. J. & Jacobs, S. J. Chemistry of detonations. I. A simple method for calculating detonation properties of C–H–N–O explosives. *J. Chem. Phys.* **48**, 23–35 (1968).
39. Zhang, Q. et al. Prediction of detonation pressure and velocity of explosives with micrometer aluminum powders. *Cent. Eur. J. Energetic Mater.* **9**, 77–86 (2012).
40. Xia, K. et al. Pressure-stabilized high-energy-density alkaline-earth-metal pentazolate salts. *J. Phys. Chem. C* **123**, 10205–10211 (2019).
41. Keshavarz, M. H. & Pouretedal, H. R. Predicting detonation velocity of ideal and less ideal explosives via specific impulse. *Indian J. Eng. Mater. Sci.* **11**, 429–432 (2004).
42. Wang, H. et al. CALYPSO structure prediction method and its wide application. *Comput. Mater. Sci.* **112**, 406–415 (2016).
43. Dunnington, B. D. & Schmidt, J. R. Generalization of natural bond orbital analysis to periodic systems: applications to solids and surfaces via plane-wave density functional theory. *J. Chem. Theory Comput* **8**, 1902–1911 (2012).
44. Blöchl, P. E. Projector augmented-wave method. *Phys. Rev. B* **50**, 17953–17979 (1994).
45. Parr, R. G. Density functional theory. *Ann. Rev. Phys. Chem.* **34**, 631–656 (1983).
46. Thonhauser, T. et al. Spin signature of nonlocal correlation binding in metal-organic frameworks. *Phys. Rev. Lett.* **115**, 136402 (2015).
47. Maintz, S., Deringer, V. L., Tchougreeff, A. L. & Dronskowski, R. Analytic projection from plane-wave and PAW wavefunctions and application to chemical-bonding analysis in solids. *J. Comput. Chem.* **34**, 2557–2567 (2013).
48. Dronskowski, R. Crystal Orbital Hamilton Populations (COHP): energy-resolved visualization of chemical bonding in solids based on density-functional calculations. *J. Phys. Chem. A* **97**, 8617–8624 (1993).
49. Togo, A., Oba, F. & Tanaka, I. First-principles calculations of the ferroelastic transition between rutile-type and  $CaCl_2$ -type  $SiO_2$  at high pressures. *Phys. Rev. B* **78**, 134106 (2008).

## Acknowledgements

This work was supported by the National Key R&D Program of China (2018YFA0703404), National Key Research and Development Program (No. 2017YFA0403704), National Natural Science Foundation of China (Nos. 91745203, 11404134, 11574109, 11474127, and 11674122), National Key Research and Development Program of China (2016YFB0201204). Program for Changjiang Scholars and

Innovative Research Team in University (No. IRT\_15R23), National Found for Fostering Talents of basic Science (No. J1103202), Parts of calculations were performed in the High Performance Computing Center (HPCC) of Jilin University.

## Author contributions

D.L. designed this project. Z.L., Q.Z., F.T., D.D., and F.L. analyzed the data; Z.L., D.L., and T.C. made the analysis and wrote the paper. All authors discussed the results and commented on the paper.

## Competing interests

The authors declare no competing interests.

## Additional information

Supplementary information is available for this paper at <https://doi.org/10.1038/s42004-020-0286-1>.

Correspondence and requests for materials should be addressed to D.L. or T.C.

Reprints and permission information is available at <http://www.nature.com/reprints>

**Publisher's note** Springer Nature remains neutral with regard to jurisdictional claims in published maps and institutional affiliations.



**Open Access** This article is licensed under a Creative Commons Attribution 4.0 International License, which permits use, sharing, adaptation, distribution and reproduction in any medium or format, as long as you give appropriate credit to the original author(s) and the source, provide a link to the Creative Commons license, and indicate if changes were made. The images or other third party material in this article are included in the article's Creative Commons license, unless indicated otherwise in a credit line to the material. If material is not included in the article's Creative Commons license and your intended use is not permitted by statutory regulation or exceeds the permitted use, you will need to obtain permission directly from the copyright holder. To view a copy of this license, visit <http://creativecommons.org/licenses/by/4.0/>.

© The Author(s) 2020